Journal of Marine Systems 82 (2010) 295–303

Contents lists available at ScienceDirect

Journal of Marine Systems

journal homepage: www.elsevier.com/locate/jmarsys

Observations of chromophoric dissolved and detrital organic matter distribution using remote sensing in the Southern Ocean: Validation, dynamics and regulation

E. Ortega-Retuerta [a,b,*], D.A. Siegel [c], N.B. Nelson [c], C.M. Duarte [d], I. Reche [a,e]

[a] Departamento de Ecología, Facultad de Ciencias, Universidad de Granada, 18071, Spain
[b] CNRS, UMR 7621, LOMIC, Observatoire Océanologique, F-66651, Banyuls/mer, France
[c] Institute for Computational Earth System Science, University of California Santa Barbara, CA 93106-3060, USA
[d] Department of Global Change Research, IMEDEA (CSIC-UIB) Instituto Mediterráneo de Estudios Avanzados, Miquel Marqués 21, 07190 Esporles, Spain
[e] Instituto del Agua, Universidad de Granada, 18071, Spain

ARTICLE INFO

Article history:
Received 18 January 2010
Received in revised form 4 June 2010
Accepted 10 June 2010
Available online 1 July 2010

Keywords:
Chromophoric dissolved organic matter
Detrital absorption
Ocean color
Remote sensing
Antarctic peninsula
Southern ocean

ABSTRACT

Chromophoric dissolved and detrital organic matter (CDM), the optically active fraction of organic matter, affects significantly the underwater light environment and interferes with ocean color algorithms. Here, we studied the distribution and dynamics of CDM in waters around the Antarctic Peninsula, Southern Ocean, using remotely sensed data in austral summers from 1997 to 2005. First, we validated the global semi-analytic algorithm Garver–Siegel–Maritorena (GSM) by comparing simultaneous field and satellite measurements of CDM. These comparisons confirmed the validity of CDM satellite measurements obtained by the GSM algorithm ($r^2 = 0.74$, slope value $= 1.01 \pm 0.16$, $n = 15$).We found a higher (20%) contribution of detrital particles to the CDM signal compared to other studies in lower latitudes (average 12%). Patches of higher CDM were observed in coastal areas and zones with recent ice melting. The seasonal variability of CDM, with maximum values at the end of austral summer, appeared to be ultimately controlled by the dynamics of ice, both directly and indirectly through the growth of phytoplankton and other organisms which are potential sources of CDM. At an interannual timescale, CDM dynamics may be driven by climatic forcing such as the Antarctic Oscillation.

1. Introduction

Chromophoric dissolved organic matter (CDOM) quantifies the absorption of the light-absorbing fraction of the dissolved organic matter pool (Nelson and Siegel, 2002; Coble, 2007). The increased interest in the study of CDOM in marine ecosystems is related to its role attenuating solar radiation and affecting ocean color algorithms (Siegel et al., 2002; 2005a). CDOM regulates the intensity and spectral quality of light for photosynthesis also protects organisms from UV damage (Arrigo and Brown, 1996; Williamson et al., 2001) and plays an important role in the heat budget of the ocean (Claustre and Maritorena, 2003). In addition, these compounds are related in the cycling of carbon and other elements as they mediate photochemical reactions (Mopper et al., 1991). These reactions would involve changes in the optical properties and lability of DOM (Mopper et al., 1991; Kieber et al., 1997; Benner and Biddanda, 1998), the release of secondary products (e.g. inorganic carbon forms and reactive oxygen species) (Blough and Zepp, 1995), or the alteration or the redox state of metals (Mopper et al., 1991). Although CDOM only refers to absorption of dissolved compounds, satellite measurements generally measure the combined absorption of CDOM and detrital particles together as they are spectrally similar (e.g., Siegel et al., 2002). We thus refer to CDM as absorption of dissolved and detrital organic matter measured at 443 nm.

In the Southern Ocean, there are several important reasons for studying CDOM dynamics. First, the Southern Ocean is subject to extreme solar radiation in the austral summer. During this time, photochemical reactions involving CDOM are significant (Ortega-Retuerta et al., 2010). Second, CDOM in high latitudes is abundant, and, in fact, accounts for up to 70% of the total non-water light absorption at 443 nm (Siegel et al., 2002). Hence, at these latitudes CDOM may play a crucial role in light attenuation and light ability to photosynthesis. Recent reports of rates of photochemical reactions from the Southern Ocean are substantially higher than in temperate waters and are attributed to high ambient nitrate concentrations interacting with the CDOM pool (Toole et al., 2008). However, the knowledge of CDOM dynamics in the Southern Ocean is still insufficient and restricted to short-term studies.

Satellite remote sensing allows the retrieval of ocean optical properties over wide areas of the ocean and the ability to collect long data series of remote locations. Initially, remote sensing of ocean color focused on the retrieval of the concentration of chlorophyll *a* (chl *a*).

* Corresponding author. Current address: UPMC Univ Paris 06, UMR 7621, LOMIC, Observatoire Océanologique, F-66651, Banyuls/mer, France.
E-mail address: ortega@obs-banyuls.fr (E. Ortega-Retuerta).

0924-7963/$ – see front matter © 2010 Elsevier B.V. All rights reserved.
doi:10.1016/j.jmarsys.2010.06.004

However, remote sensing of ocean color is increasingly delivering a wider range of products, including data on other inherent optical properties (IOCCG, 2006). There are two kinds of bio-optical algorithms employed to retrieve inherent optical properties (i.e. pigments absorption, the combined absorption due to CDOM and detrital particulate matter (CDM), and particle backscattering coefficients) from satellite radiance observations: empirical and semi-analytic algorithms. Empirical algorithms assume that inherent optical properties can be predicted from a measure of water-leaving radiance, $L_{wN}(\lambda)$, or a ratio of $L_{wN}(\lambda)$ values, in a predictable manner. This assumption is not always valid (Siegel et al., 2005a). By contrast, semi-analytic algorithms, such as the Garver–Siegel–Maritorena (GSM) model (Maritorena et al., 2002), discriminate the relative contribution of the different non-water optical constituents. The GSM model was optimized using a large global *in situ* dataset (Siegel et al., 2002; Gregg and Casey, 2004; Siegel et al., 2005a) and although its robustness has been addressed at global scales (Siegel et al., 2005a; Maritorena et al., 2010), this has not as yet been demonstrated for the Southern Ocean.

In the Southern ocean, global empirical algorithms generally underestimate chlorophyll concentration (McClain, 2009). The proposed reasons for this discrepancy are low chlorophyll specific absorption (Mitchell and Holmhansen, 1991; Dierssen and Smith, 2000), low backscattering of particles (Dierssen and Smith, 2000), different approaches used for estimating chl *a* (Marrari et al., 2006) or differences in the composition of the algal community (Arrigo et al., 1998). As empirical algorithms use a fixed relation between water-leaving radiance and chl *a*, a different ratio between chlorophyll *a* and CDM may also account for this error (Siegel et al., 2005b). Validation of satellite chl *a* measurements have been conducted repeatedly from the Southern Ocean (Reynolds et al., 2001; Gregg and Casey, 2004; Moore and Doney, 2006); however there are, to the best of our knowledge, no studies comparing remotely sensed CDM data to field observations.

Here we apply satellite remote sensing observations to assess the dynamics and controls on the CDM distribution in the Southern Ocean in and around the Antarctic Peninsula. First, we validate the GSM algorithm using available field data. Then, we apply these satellite-based observations to assess geographical variability and temporal dynamics of CDM in this area. Last, we explore the potential driving factors and show the influence that climate oscillators have on the CDM distribution.

2. Material and methods

2.1. Validation of GSM data of CDM with field CDOM data

To validate the GSM model for remote sensing measurements of CDM in the Southern ocean, we compared satellite data with field observations of CDOM and detrital absorption from three different datasets:

(1) CDOM and detrital data corresponding to austral summers of 1997, 1998 and 1999 were obtained from the Palmer Long Term Ecological Research (PalLTER) dataset (e.g., Ducklow, 2008 — DSR2 special issue editorial; http://pal.lternet.edu/). The Palmer LTER site is centered at the U.S. research station Palmer on Anvers Island (Fig. 1, 64°40′ S 64°03′ W). The dataset covers a grid situated west of the Antarctic Peninsula that extends over a region of 900 km^2 with sampling points spaced every 20 km, roughly parallel with the peninsula. CDOM spectra were measured from filtered samples (polycarbonate filters, 0.2 μm) using 10 cm path length quartz cuvettes in a Perkin-Elmer Lambda 6 spectrophotometer (Patterson, 2000). Detrital absorption was measured in GF/F filters after pigment removal by methanol extraction following standard protocols (Kishino et al., 1985; Pegau et al., 2003). Chlorophyll *a* was measured fluorometrically in GF/F filters with methanol extraction according to standard protocols (Holm-Hansen and Riemann, 1978).

(2) CDOM and detrital data for the years 2000, 2001 and 2002 were obtained from the SeaBass ocean optics data archive (http://seabass.gsfc.nasa.gov/). The SeaBass data archive was created to support regular scientific analyses (satellite data product validation, algorithm development and other scientific goals), such as bio-optical data for validation of satellite ocean color data. The specific data used here corresponded to AMLR cruises (PI Dr. Greg Mitchell) during February–March 2000, 2001 and 2002 along the Gerlache Strait and South Shetland Islands (Fig. 1). CDOM was measured from filtrate samples (0.2 μm) according to the standard protocols (Pegau et al., 2003). Detrital absorption was measured in GF/F filters after pigment removal by methanol extraction following standard protocols (Kishino et al., 1985; Pegau et al., 2003).

(3) CDOM dataset corresponding to 2004 and 2005 were obtained during ICEPOS cruises in the Antarctic Peninsula. CDOM was measured from filtered samples (Whatman GF/F, ≈0.7 μm) using 10 cm path length quartz cuvettes in a Shimadzu UV-2401 PC (more details in Ortega-Retuerta et al., 2010). Chlorophyll *a* was measured fluorometrically in GF/F filters with methanol extraction according to standard protocols (Holm-Hansen and Riemann, 1978).

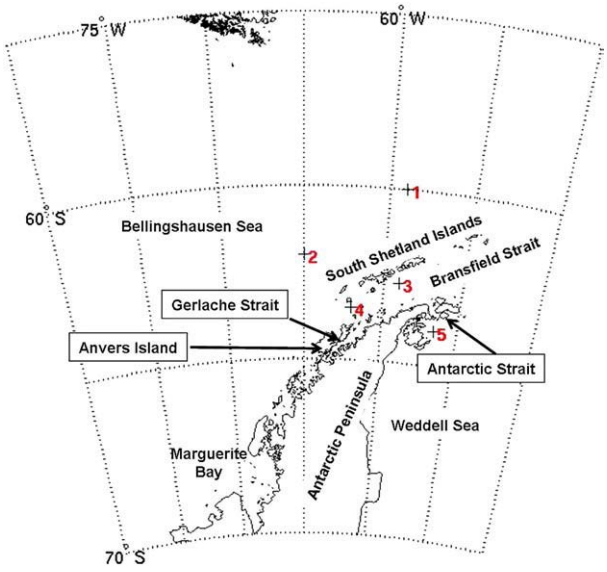

Fig. 1. The area of the Antarctic Peninsula where this study was performed. The numbers from 1 to 5 indicate the selected locations for the temporal dynamics.

To account for the contribution of detrital absorption to the sum of chromophoric dissolved and detrital absorption (CDM), we calculated its percent contribution as follows:

$$\%a_{det} = \frac{a_{det}(443)}{a_{cdom}(443) + a_{det}(443)} \times 100 \quad (1)$$

where $a_{cdom}(443)$ is the absorption by chromophoric dissolved organic matter and $a_{det}(443)$ is the absorption of detrital particles, both measured at 443 nm.

Satellite CDM observations were obtained from SeaWIFS data from 1997 to 2002 and from merged (SeaWIFS + MODIS-Aqua) data from 2002 to 2005 corresponding to GSM products on 9×9 km grids in daily and monthly averages (http://wiki.icess.ucsb.edu/measures/index.php/GSM; Maritorena et al., 2010). Briefly, the GSM semi-analytical ocean color model (Maritorena et al., 2002) is based on the

relationship between water-leaving radiance ($L_{wN}(\lambda)$) and important inherent optical properties (IOPs), which are decomposed into absorption by phytoplankton (a_{ph}), chromophoric dissolved and detrital organic matter (a_{cdm}) and pure water (a_w), and backscattering of water (b_{bw}) and particles (b_{bp}). The GSM algorithm assumes that the spectral shapes of these IOPs are fixed and their magnitudes are allowed to vary resulting in three unknowns to be determined:

$$L_{WN}(\lambda) = \left(\frac{tF_0(\lambda)}{n^2\, sw}\right)\sum_{m=1}^{2} g_m \times\left\{\frac{b_{bw}(\lambda) + BBP(\lambda_0/\lambda)^{\eta}}{b_{bw}(\lambda) + BBP(\lambda_0/\lambda)^{\eta} + a_w(\lambda) + Chl^{*}_{a_{ph}}(\lambda) + CDMexp[-S(\lambda-\lambda_0)]}\right\}^{m} \quad (2)$$

where BBP (particulate backscattering), chl (chlorophyll *a*) and CDM (chromophoric dissolved and detrital matter) are the unknown IOP amplitudes to be retrieved.

GSM and field data matchups were validated following the protocol described in Bailey and Werdell (2006). Daily satellite observations were obtained from a 3×3 pixel grid centered in the location of the field data point. We only used GSM data with more than 4 pixels with valid data. Data from all valid pixels in the 3×3 matrix were averaged and compared with the corresponding field data points.

2.2. Spatial distribution and temporal dynamics of CDM around Antarctic Peninsula

To evaluate spatial and temporal variability of CDM and its potential drivers, maps of satellite data corresponding to the Antarctic Peninsula area (from 55 to 70° S and from 50° to 80° W) were clipped from the global GSM mapped imagery.

To examine CDM temporal dynamics we selected five locations with contrasting properties (Table 1). Locations 1 and 2 are situated in offshore waters west of the Antarctic Peninsula, locations 3 and 4 are situated along the coastline in the Bransfield Strait region, and location 5 is situated in the northern Weddell Sea near the Antarctic Strait (Fig. 1).

To evaluate interannual variability in CDM dynamics we calculated monthly CDM anomalies using the following expression:

$$\text{CDM Anomaly}(\%) = \frac{a_{cdm}(443)_a - \overline{a_{cdm}(443)_a}}{\overline{a_{cdm}(443)_a}} \times 100 \quad (4)$$

where $a_{cdm}(443)_a$ is the monthly CDM in a single month and $\overline{a_{cdm}(443)_a}$ is the average CDM for the same month over all years (1997–2005). Positive values represent higher CDM concentration than usual and vice versa.

2.3. Spatial and temporal drivers of CDM around Antarctic Peninsula

We used satellite data of different geophysical variables from different sources to evaluate the potential controlling factors of CDM distribution and dynamics. Chl *a* data were also obtained from SeaWIFS (1997–2002) or merged (2002–2005) using the GSM products (http://wiki.icess.ucsb.edu/measures/index.php/GSM). Sea surface temperature (SST) data were obtained from NOAA/NASA AVHRR Pathfinder Global 9 km daily SST Products averaged over monthly periods (http://podaac.jpl.nasa.gov/DATA_CATALOG/avhrr.html). Photosynthetically active radiation (PAR) satellite data (E m^{-2} d^{-1}) from SeaWIFS, were obtained from the NASA's Ocean Color database (http://oceancolor.gsfc.nasa.gov/DOCS/seawifs_par_wfigs.pdf). Ice concentration data, as percentage of the area covered by sea ice on 25 km pixels, were obtained by DMSP SSM/I passive microwave data from the National Snow and Ice Data Center (Boulder, Colorado USA) (http://nsidc.org/data/).

The Antarctic Oscillation Index (AAO, also known as southern annular mode, SAM) was used as an indicator for climatic conditions relevant to the Antarctic Peninsula (Thompson and Solomon, 2002). Monthly values of the AAO index were obtained from the Climate Prediction Center of the NOAA's National Weather Service (http://www.cpc.noaa.gov/products/precip/CWlink/daily_ao_index/aao/aao.shtml). AAO is defined as the difference of zonal mean sea level pressure between 40° S and 65° S and it is used as an objective index to monitor and measure the atmospheric circulation condition in high southern latitudes. AAO positive anomaly values are associated with a lowering of geopotential heights over Antarctica and an increasing strength of the westerlies over the subpolar Southern Ocean (Thompson and Solomon, 2002), with positive AAO values generally coinciding with positive anomalies of sea surface temperature and higher ice retreat in the Antarctic Peninsula area (Hall and Visbeck, 2002; Justino and Peltier, 2008; Meredith et al., 2008).

Table 1
Geographical coordinates (latitude and longitude) and means of ($a_{cdm}(443)$, m^{-1}), chl *a* (mg m^{-3}), sea surface temperature (°C) and photosynthetically active radiation (E m^2 d^{-1}) for the five selected locations.

Location	1	2	3	4	5
Lat (°)	−60	−62	−62.7	−63.5	−64
Lon (°)	−59	−65	−59	−62	−56.5
$a_{cdm}(443)$	0.013	0.014	0.022	0.022	0.036
Chlorophyll *a*	0.11	0.13	0.29	0.28	0.65
Sea surface temperature	na	1.88	0.91	0.71	−0.01
Photosynthetically active radiation	26.1	25.0	27.9	22.6	26.1

3. Results

3.1. Validation of GSM CDM data with field CDOM data

A total of 142 field observations of CDOM were available for validating the GSM retrievals; however only 15 field observations were collected simultaneously with clear-sky satellite observations. These field data belonged to Palmer LTER (1 matchup) and AMLR cruises (14 matchups). A good correspondence was found between field $a_{cdom}(443)$ and satellite GSM $a_{cdm}(443)$ observations ($r^2 = 0.70$, $n = 15$). The relationship between field and GSM data showed a slope of 1.24 ± 0.23 which is significantly greater than one (Fig. 2A). The detrital absorption $a_{det}(443)$, determined in Palmer and AMLR datasets, contributed a mean 19% to the *in situ* $a_{cdm}(443)$. When comparing field CDM ($a_{det}(443) + a_{cdom}(443)$) with GSM $a_{cdm}(443)$, a significantly better fit was achieved, including a slope of nearly one ($r^2 = 0.75$, slope value = 1.01 ± 0.16, Fig. 2A). These results demonstrate that the GSM algorithm provides consistent retrievals of CDM in the Antarctic Peninsula.

The 19 valid matchups obtained between *in situ* and GSM chlorophyll *a* concentration were found in the AMLR dataset. Although a high value of explained variance was obtained for the *in situ*-satellite relationship ($r^2 = 0.83$, Fig. 2B), the slope value (0.24) was significantly lower than 1, implying an underestimation of chlorophyll *a* values in the area when applying the GSM algorithm.

3.2. Spatial distribution and temporal dynamics of CDM around Antarctic Peninsula

The GSM results allow the visualization of the monthly CDM distribution in the Antarctic Peninsula area during ice-free periods (from September to April). Monthly averages were used to help complete spatial coverage off the Antarctic Peninsula. The monthly CDM distributions showed higher values near the coastlines or in zones with recent ice melting, particularly in Marguerite Bay

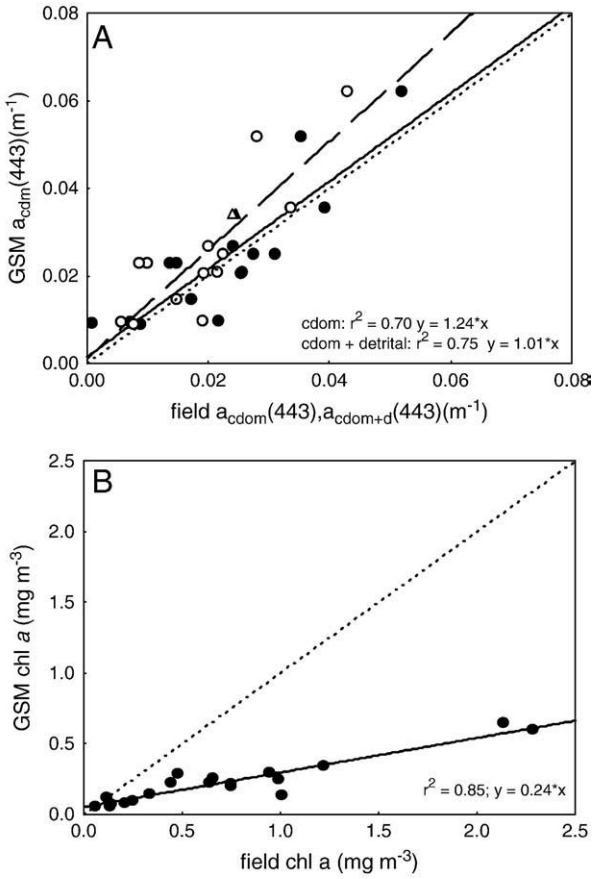

Fig. 2. (A) Results of direct comparisons between *in situ* $a_{cdom}(443)$ and GSM satellite $a_{cdm}(443)$ (open symbols, dashed line) and between *in situ* $a_{cdom} + a_d(443)$ and GSM satellite $a_{cdm}(443)$ (continuous line, filled symbols). Dotted line represents slope = 1. Triangles: Data from Palmer LTER. Circles: Data from AMLR cruises. (B) Results of direct comparisons between *in situ* chl *a* and GSM satellite chl *a*. Dotted line represents slope = 1. All data (circles) correspond to AMLR cruises.

(Southwestern Antarctic Peninsula), in the Western Weddell Sea below the Antarctic strait, along the Peninsula coastline, and near South Shetland Islands in the Bransfield strait (Fig. 3).

At the beginning of the ice-free period (October–November), the CDM values were lower than 0.1 m^{-1} at all locations. However as the austral summer progressed, we observed a more contrasting CDM geographical pattern between shore and offshore locations (Fig. 3). In February–March, CDM reached absorption up to 0.73 m^{-1} (pixels with highest values in the monthly CDM maps) in areas near the coastline and adjacent to the ice edge. This pattern from homogenous to patchy pictures, although variable in absolute concentrations, was consistent in all studied ice-free periods.

The five selected locations show a range of CDM dynamics (see Table 1 and Fig. 1 for their locations). For example, for location 5 (situated near the ice boundary in the Weddell Sea), we found the highest CDM values (mean CDM = 0.036 m^{-1}); whereas for locations 1 and 2 (situated in open waters), CDM values were comparatively lower (mean CDM = 0.013 m^{-1}; see Table 1).

For locations 1 and 2, the highest CDM values were observed in the austral spring months (November–December). In contrast, highest CDM was observed during the austral summer (January–March) at locations 3, 4 and 5 (Fig. 4). The seasonal amplitude was also variable among locations (Fig. 4). CDM values oscillated seasonally in a range of 0.015 to 0.033 m^{-1} between maxima and minima at stations 1, 2, 3 and 4. By contrast, the observed seasonal amplitude at location 5 was much higher (0.099 m^{-1}; Fig. 4).

The determination of temporal patterns of the CDM anomaly let us to diagnose interannual variability and these changes may differ among the selected locations. Locations 1 and 2 (which are relatively far from the coastline) showed small, rather uniform values of the CDM anomaly with comparatively little variability. By contrast, locations inside the Bransfield Strait (3 and 4) showed variations of the CDM anomaly ~40% with a cyclic pattern where negative anomalies are found from 1997 to 1999 and from 2002 to 2004 with positive anomalies from 2000 to 2001 and in 2005 (Fig. 5). Finally location 5, situated in the western Weddell Sea, showed very large CDM anomalies (±100%) (Fig. 5). Its temporal pattern was quite irregular, with positive anomalies observed in the same periods as in locations 3 and 4, being highest in 2005 (Fig. 5).

3.3. Spatial and temporal drivers of CDM around Antarctic Peninsula

Correlation coefficients between CDM and chl *a* were significant and positive for all five locations (Table 2). Values of SST were weakly correlated with CDM, being only positively related inside the Bransfield Strait (location 3). CDM and PAR were positively correlated only at the Southern locations (3, 4 and 5), and this correlation was particularly high at location 5 in the Weddell Sea (Table 2). Finally, for the locations situated nearer the ice boundary layer (sites 3 to 5), CDM was negatively correlated to ice concentration, while not significant correlations were obtained at locations 1 and 2 (Table 2).

At a monthly temporal resolution, changes in CDM and chl *a* were synchronous at the 5 sites with no lagged response, which would indicate that one which was the precursor of the other, was detected between these variables ($p > 0.05$). For the monthly data examined, significant lagged correlations were not observed in any study locations and years. Regions of elevated chl *a* and CDM also coincided geographically, which could be visualized when comparing monthly satellite images of CDM and chl *a* (Fig. 6).

Likewise, CDM anomalies were correlated with chl *a* for all five locations (Table 2), and the CDM anomaly was related to AAO at locations 1 and 2 (Table 2) but not significantly correlated to SST, PAR at any locations and with ice concentration only at location 5. The oscillation pattern of the AAO index was similar to that of the CDM anomaly. Periods with positive CDM anomalies roughly corresponded to positive AAO and vice versa, except from spring and summer 2000–2001. For station 5 we did not obtain significant correlations, but similar trends between the CDM anomaly and AAO could be observed (Fig. 5).

4. Discussion

4.1. Validation of GSM CDM data with field CDOM data

The validity of the GSM algorithm in the Antarctic Peninsula was confirmed in this study as significant comparisons between field observations and satellite data (GSM model) were obtained. Indeed, the GSM model, which has been optimized for global open ocean waters, has also reported satisfactory results when applied to more optically complex coastal waters (Kudela and Chavez, 2004; Magnuson et al., 2004; Kostadinov et al., 2007).

The slope of the regression equation between field $a_{cdom}(443)$ and GSM $a_{cdm}(443)$ was higher than the regression lines obtained globally (Siegel et al., 2002; Siegel et al., 2005a). The comparative analysis was made between field CDOM (0.2 μm filtered water) and satellite CDM data also including absorption due to detrital particulate matter (i.e. the fraction retained by GF/F filters). The higher slope values for the field $a_{cdom}(443)$–GSM $a_{cdm}(443)$ than those reported by Siegel et al. (2002) for the global ocean suggest a higher contribution of detrital particles to CDM absorption in this particular area. This contribution averaged 20%, in contrast to a mean 12% in the Sargasso Sea (Siegel et al., 2002). This higher contribution of detrital material could be caused by ice meltwater during austral summer, that has a noticeable influence from the ice edge to waters up to 100 km offshore, and particles release "glacial flour",

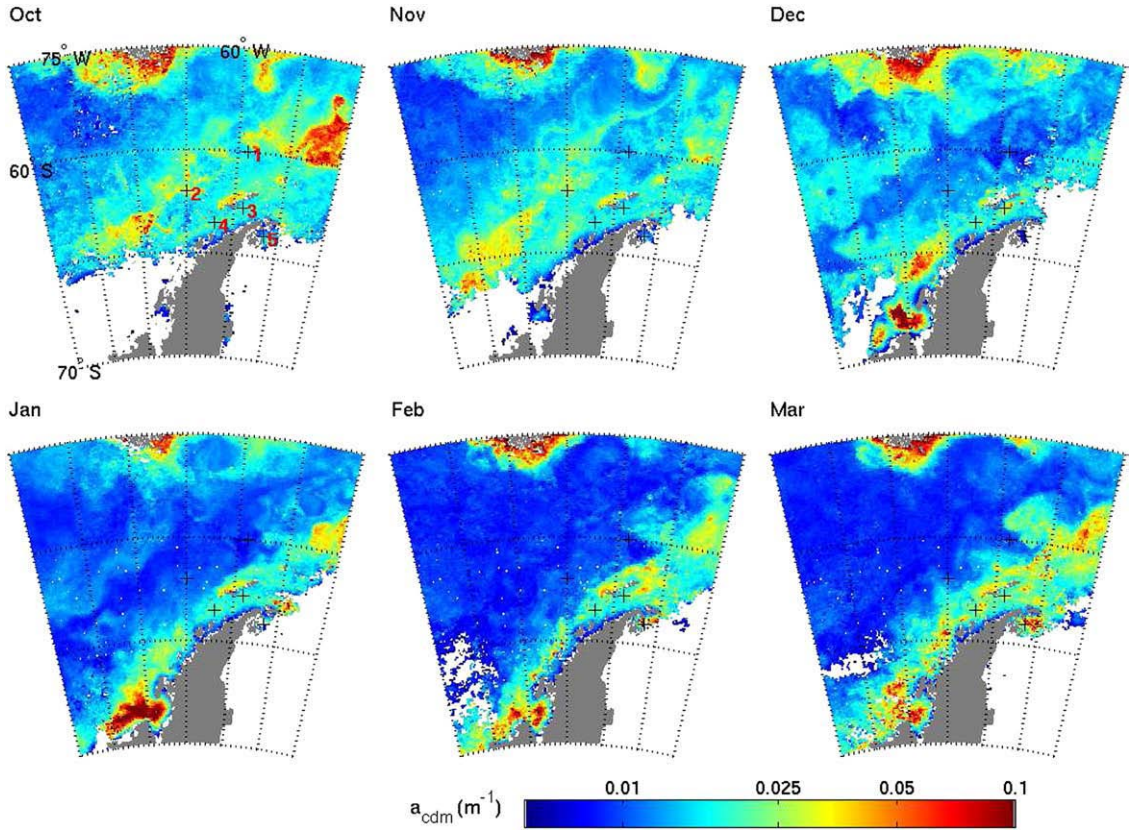

Fig. 3. Maps of CDM ($a_{cdm}(443)$, m^{-1}) in the Antarctic Peninsula area during 2003–2004 period (from October to March) with a spatial coverage of 9 × 9 km pixel grid. White areas represent locations with no valid data over the entire month. Wide white areas at the bottom of the figures represent zones covered by ice.

silicious particles released with glacial discharge (Dierssen et al., 2002) and other meltwater-released particles. Indeed, if the comparison includes field detrital absorption ($a_d(443)$) the obtained a slope value is approximately one, confirming the validity of the GSM algorithm for CDM retrievals in the area (Fig. 2).

In contrast to the validity of the GSM algorithm for CDM retrieval, the comparison of *in situ* chlorophyll *a* values with those obtained by satellite using the GSM algorithm resulted in an underestimation of chlorophyll *a* concentrations, consistent with previous studies (Mitchell and Holmhansen, 1991; Dierssen and Smith, 2000; Marrari et al., 2006). This result suggest that a difference in relative contribution of CDM and chlorophyll *a* to $L_W(\lambda)$ would not explain these biases, as the GSM algorithm retrieves CDM and chlorophyll *a* data in an independent way. Hence, the underestimation of chlorophyll *a* in this region is more likely due to other reasons such as different pigment-specific absorption (Mitchell and Holmhansen, 1991; Dierssen and Smith, 2000), phytoplankton composition (Arrigo et al., 1998), or methodology (Marrari et al., 2006). Indeed, a previous study (Marrari et al., 2006) proposes the use of global algorithms to retrieve valid chlorophyll *a* data in the area, while the biases would reside in field fluorescence measurements that overestimate chlorophyll *a* concentration. Although the validity of absolute chlorophyll *a* concentrations retrieved using the GSM algorithm is not clear, we used these data to compare chlorophyll *a* and CDM dynamics as their seasonal and spatial patterns are likely independent on absolute chl *a* values.

4.2. Spatial and temporal dynamics of CDM around Antarctic Peninsula and driving factors

Satellite observations of the CDM distribution enabled us to observe non-uniformity in the CDM distribution. Patches of higher CDM are found in coastal areas and zones with recent ice melting during the austral summer. We could see, however, narrow areas adjacent to the ice boundary where CDM absorption exhibited low values (i.e. $a_{cdm}(443) < 0.01\ m^{-1}$, see Fig. 3). This fact is likely due to adjacency effect, which leads to underestimation of IOPs when applying ocean color algorithms in areas located up to 20 km from the ice edge (Belanger et al., 2007). Thus, data corresponding to pixels located within this distance to the ice edge are likely biased and should be taken with caution. Although the general distribution pattern of CDM was observed in all the study ice-free periods, the specific areas with higher ice retreat were variable among the different periods. The study of CDM anomalies in single locations revealed that CDM dynamics for some regions are regulated not only by seasonal drivers (i.e. dynamics of ice and biological communities), but also by interannual climatic forcings such as the variation in the Antarctic Oscillation (AAO) Index.

Regions of high CDM in the coastal areas or the ice edge are not likely associated with increases in terrestrial inputs of dissolved organic matter due to river discharges and are more likely created by snow and glacial ice melting from land or to sea ice retreat (Dierssen et al., 2002). Indeed for the locations situated near the coastline of the Antarctic Peninsula or the ice edge showed higher average seasonal CDM ranges and amplitudes than offshore locations, especially later in the season (Fig. 4). In areas with mixed ice and seawater, CDM can be overestimated due to sub-pixel contamination (Belanger et al., 2007; Wang and Shi, 2009). In our study locations, however, highest CDM values were observed in those months when ice concentration was very low (<5% in a 25 km pixel) or absent, while those periods with high ice concentration generally (particularly in location 5) coincided with no valid CDM data. For locations 3 to 5, a negative correlation between ice concentration and CDM was observed. Further work is needed to accurately estimate the magnitude of CDM attributable to ice melting dynamics.

Temperature is a primary controlling factor of all metabolic processes (Pomeroy and Wiebe, 2001; Boyd, 2002) and, thus, it

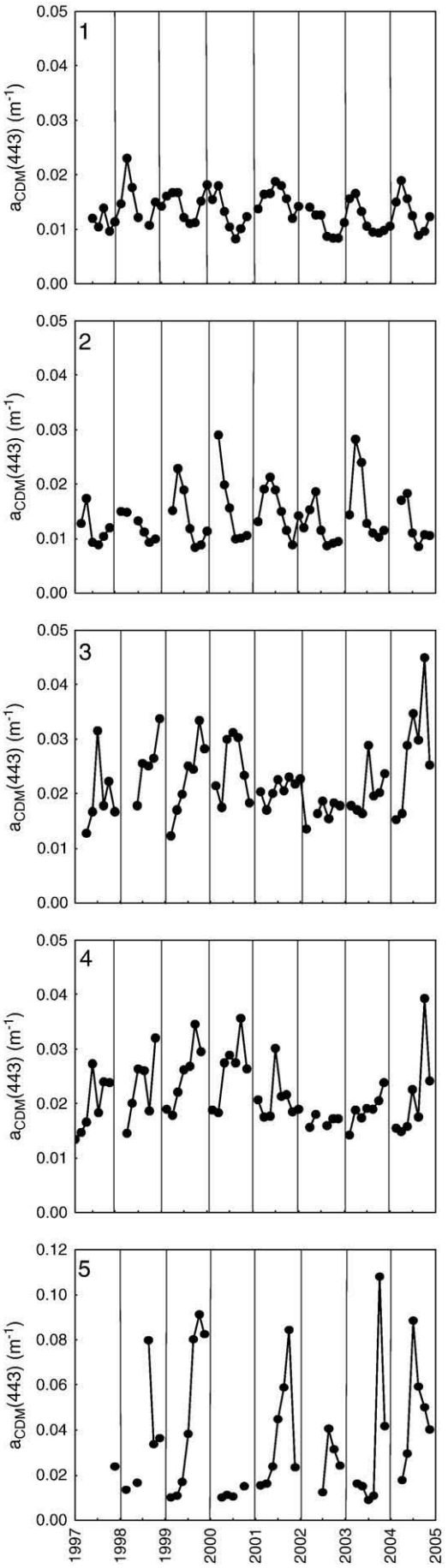

could regulate biological CDOM generation and consumption processes. However, monthly variations in sea surface temperature appeared not to be a major driver of CDM in this region as no consistent relationships were encountered between CDM and SST (except for location 3, Table 2).

Photobleaching losses represent an important sink of CDOM in the ocean surface (Vodacek et al., 1997; Nelson et al., 1998). A negative correlation between solar radiation (here PAR) and CDOM would be expected if PAR radiation contributes to CDOM photobleaching at 440 nm (Reche et al., 2000). In contrast, these two variables were positively correlated in the locations situated at higher latitudes. This fact could be partly due to an indirect effect of CDOM generation through an enhancement of primary production by PAR in these higher latitudes with light limitation (Mitchell et al., 1991; Boyd, 2002). Hence, in this area and temporal scale, PAR radiation light alone does not act apparently as a primary net sink for CDM.

The positive relationship between CDM and chl *a* was very robust (Table 2). A coincidence in CDM and chl *a* was observed both in spatial distributions and also in temporal (seasonal and interannual) dynamics (based in monthly data). The role of phytoplankton as CDM sources appears to be indirect based on previous field and experimental studies (Nelson et al., 1998; Rochelle-Newall and Fisher, 2002). One plausible explanation is that phytoplankton act as a source of CDM which is only detectable at long temporal scales (i.e. monthly averages), as all fixed carbon in the ocean has an ultimate algal source. In fact, recently Romera-Castillo et al. (2010) found CDOM production by marine phytoplankton in axenic cultures at a daily scale. The complexity of CDOM cycling, along with different turnover times of chl *a* and CDOM, uncouple and blur the relationships at shorter spatial and temporal scales (as well as for multi-decadal time scales — Nelson et al., 2007; Swan et al., 2009). In this study, the correspondence between chl *a* and CDM at monthly scales suggests that the processes converting algal DOM into CDOM should happen at a timescale of less than a month.

An alternative explanation to the synchrony between chl *a* and CDM dynamics is the similar response of both variables to external forces but by independent mechanisms (e.g., Siegel et al., 2005a). CDM values are consistently elevated in areas with recent ice retreat or in zones adjacent to the coastline, also those where blooms occur (Fig. 3). The annual advance and retreat of sea ice together with glacial meltwater dynamics are the major physical determinant of spatial and temporal changes in the structure and function of the Antarctic marine ecosystem (Dierssen et al., 2002; Ducklow et al., 2007). Sea ice and snow melting can provide macronutrients and micronutrients which were incorporated into the ice during its formation or accumulated as dust in the snow cover (Smetacek and Nicol, 2005). Therefore, an accumulation of chromophoric compounds in the ice or snow and its subsequent release during ice and snow melting would not be surprising. Although to date there are no published data, D.N. Thomas (personal comm.) measured high CDOM in ice cores from the Atlantic section of the Southern Ocean, with $a_{cdom}(440)$ in the bottom of the ice cores ranging from 0.92 to 7.60 m^{-1} (mean 4.15 m^{-1}).

The provision of macro- and micronutrients and a shallow surface layer associated to ice and snow melting can also enhance phytoplankton blooms. This can fuel other biological communities (e.g. bacterioplankton and krill) which are also sources of CDOM (Rochelle-Newall and Fisher, 2002; Nelson et al., 2004; Ortega-Retuerta et al., 2009).

The Antarctic Peninsula is one of the most vulnerable areas to global change, with a warming rate that exceeds any other observed globally (Vaughan et al., 2003; Clarke et al., 2007). This influence

Fig. 4. Temporal patterns of monthly $a_{cdm}(443)$ during the study ice-free periods (1997 to 2005) in the five selected locations. The vertical lines divide the different ice-free periods. Note that the figure corresponding to location 5 has a different scale in the y axis.

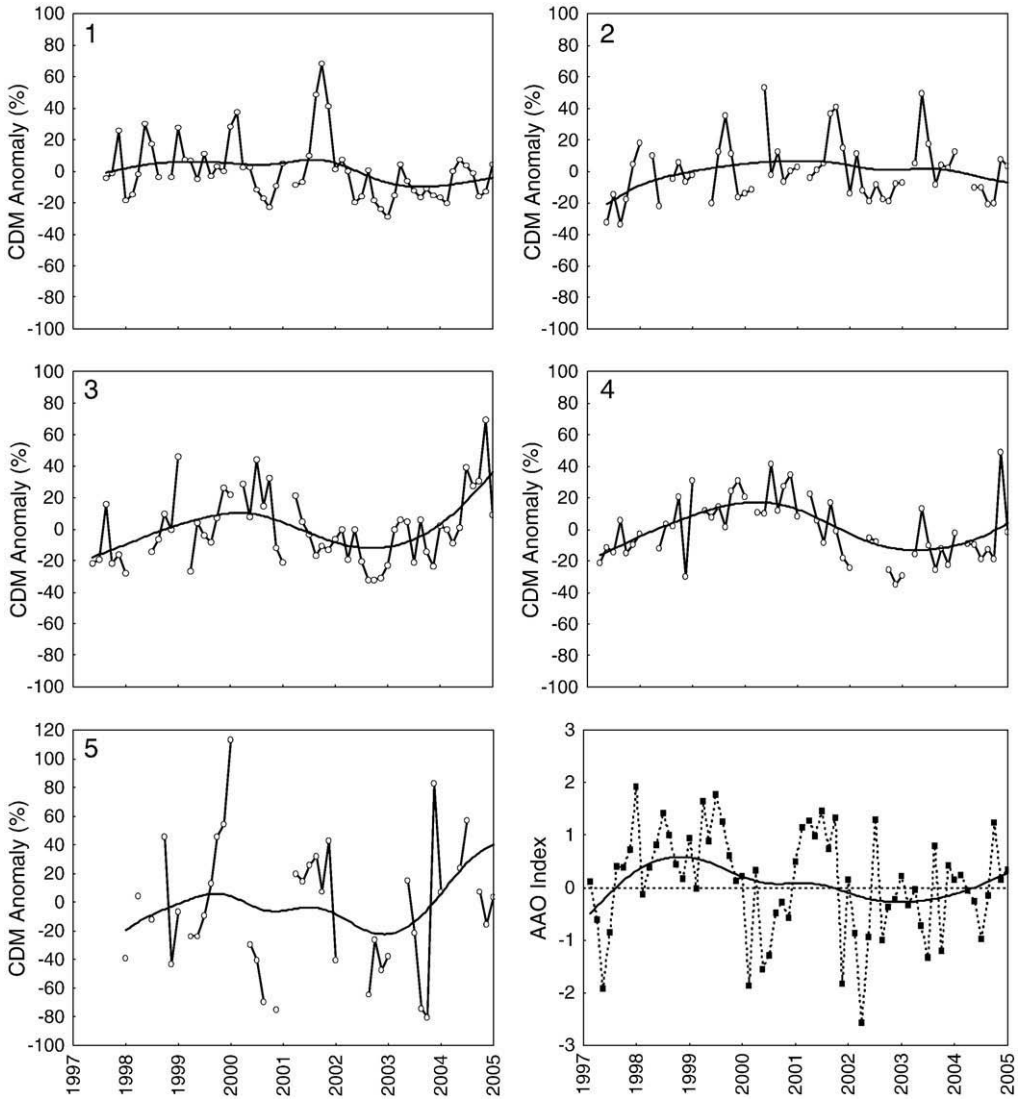

Fig. 5. Temporal patterns of monthly CDM anomalies in the five study locations (panels 1 to 5) and monthly mean of AAO Index along 1997 to 2005 ice-free periods (source: http://www.cpc.noaa.gov/products/precip/CWlink/daily_ao_index/aao/aao_index.html) in the bottom right panel. The smoothed lines correspond to the distance-weighted least squares lines.

Table 2
Correlation coefficients between chromophoric dissolved and detrital matter and chlorophyll *a* (chl *a*), sea surface temperature (SST), photosynthetically active radiation (PAR) and ice concentration, and between CDM anomalies and chl *a*, SST, ice concentration, PAR, and Antarctic Oscillation Index (AAO) in all selected locations for a sampling period between October 1997 and April 2005. Asterisks indicate significant correlations at $p<0.05$.

CDM absorption					
Location	1	2	3	4	5
Chl *a*	0.79*	0.87*	0.89*	0.83*	0.91*
SST		−0.21	0.37*	−0.27	−0.02
Ice conc.	0.17	0.05	−0.39*	−0.44*	−0.61*
PAR	−0.12	0.15	0.39*	0.27*	0.68*
CDM anomaly					
Location	1	2	3	4	5
Chl *a*	0.70*	0.42*	0.61*	0.48*	0.75*
SST	0.46*	0.25	0.02	−0.20	−0.09
Ice conc.	0.03	−0.12	−0.17	−0.14	−0.53*
PAR	0.04	0.04	−0.03	0.02	−0.05
AAO	0.32*	0.36*	−0.02	0.25	0.11

involves a significant decreasing trend in the magnitude of ice extent and in the duration of winter ice (Clarke et al., 2007; Ducklow et al., 2007) that could lead to an increase in average and seasonal amplitude of CDM. Oscillations in the Antarctic Oscillation Index (AAO) also appear to have an effect in CDM anomaly patterns (Table 2 and Fig. 5). A positive AAO index leads to an increase in CDM and vice versa. Positive anomalies of the AAO index have been associated to warmer surface temperatures and higher ice retreat in the Antarctic Peninsula area (Comiso, 2000; Kwok and Comiso, 2002; Lovenduski and Gruber, 2005) as well as higher chl *a* concentrations in the region (Lovenduski and Gruber, 2005). Under this scenario, the increase of AAO index and its consequences on physical variables such as ice extent and duration will have an evident effect on CDM concentrations altering their seasonal and interannual dynamics.

5. Conclusion

We have confirmed in this study the reliability of the GSM algorithm to retrieve CDM concentrations around Antarctic Peninsula, and highlighted the higher contribution of detrital particle absorption shown here for the Southern Ocean. The use of satellite data allowed

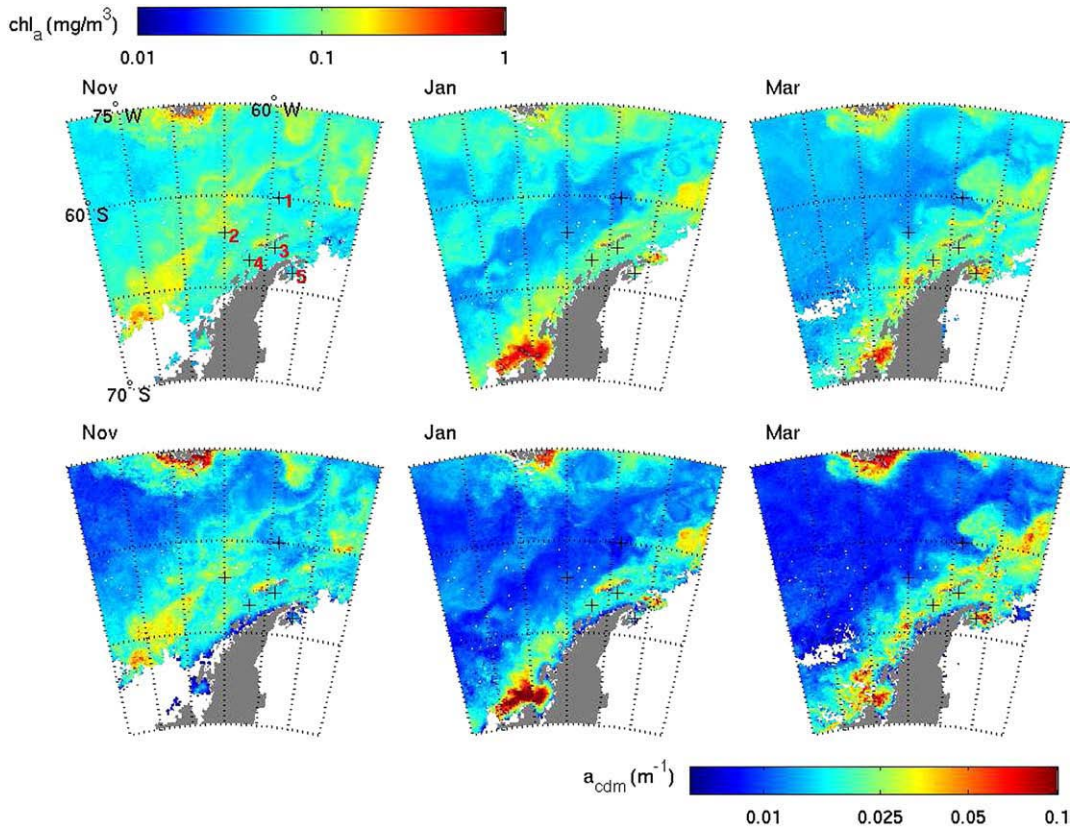

Fig. 6. Maps of CDM ($a_{cdm}(443)$, m^{-1}, bottom panels) and chl *a* (mg m^{-3}, top panels) in the Antarctic Peninsula area in November, January and March 2003–2004.

us to study geographical and temporal dynamics of CDM. We can conclude that the dynamics of sea ice and glacial snow could have a cascading effect that yield to an ultimate regulation of seasonal dynamics of CDM in the region, both directly and indirectly promoting the development of different biological communities that have a significant role in CDOM generation. At a longer timescale, CDM may also be driven by climatic forces such as the Antarctic Oscillation.

Acknowledgements

We gratefully thank K.W. Patterson and the SeaBass database, particularly B.G. Mitchell, PI of AMLR cruises, for CDOM and detrital absorption data, and D. Thomas for CDOM data on ice. AAO Index data were obtained from NOAA/National Weather Service. We also acknowledge S. Maritorena and E. Fields for assistance in data and image processing, and the responsible editor and two anonymous referees for insightful comments in a previous version of this MS. This work was funded by the Spanish Ministry of Science and Technology (ICEPOS, REN2002-04165-CO3-02 to CMD and DISPAR, CGL2005-00076 to IR) E. O.-R. was supported by fellowships from the Spanish Ministry of Science and Education and the University of Granada.

References

Arrigo, K.R., Brown, C.W., 1996. Impact of chromophoric dissolved organic matter on UV inhibition of primary productivity in the sea. Mar. Ecol. Progr. Ser. 140, 207–216.
Arrigo, K.R., Robinson, D.H., Worthen, D.L., Schieber, B., Lizotte, M.P., 1998. Bio-optical properties of the southwestern Ross Sea. J. Geophys. Res. Oceans 103 (C10), 21683–21695.
Bailey, S.W., Werdell, P.J., 2006. A multi-sensor approach for the on-orbit validation of ocean color satellite data products. Remote Sens. Environ. 102 (1–2), 12–23.
Belanger, S., Ehn, J.K., Babin, M., 2007. Impact of sea ice on the retrieval of water-leaving reflectance, chlorophyll *a* concentration and inherent optical properties from satellite ocean color data. Remote Sens. Environ. 111 (1), 51–68.
Benner, R., Biddanda, B., 1998. Photochemical transformations of surface and deep marine dissolved organic matter: effects on bacterial growth. Limnol. Oceanogr. 43 (6), 1373–1378.
Blough, N.V., Zepp, R.G., 1995. Reactive oxygen species in natural waters. In: Foote, C.S., Valentine, J.S., Greenberg, A., Liebman, J.F. (Eds.), Chemistry. Blackie, London, pp. 280–335.
Boyd, P.W., 2002. Environmental factors controlling phytoplankton processes in the Southern Ocean. J. Phycol. 38 (5), 844–861.
Clarke, A., Johnston, N.M., Murphy, E.J., Rogers, A.D., 2007. Introduction. Antarctic ecology from genes to ecosystems: the impact of climate change and the importance of scale. Philos. Trans. R. Soc. B-Biol. Sci. 362 (1477), 5–9.
Claustre, H., Maritorena, S., 2003. OCEAN science: the many shades of ocean blue. Science 302 (5650), 1514–1515.
Coble, P.G., 2007. Marine optical biogeochemistry: the chemistry of ocean color. Chem. Rev. 107 (2), 402–418.
Comiso, J.C., 2000. Variability and trends in Antarctic surface temperatures from *in situ* and satellite infrared measurements. J. Climate 13 (10), 1674–1696.
Dierssen, H.M., Smith, R.C., 2000. Bio-optical properties and remote sensing ocean color algorithms for Antarctic Peninsula waters. J. Geophys. Res. Oceans 105 (C11), 26301–26312.
Dierssen, H.M., Smith, R.C., Vernet, M., 2002. Glacial meltwater dynamics in coastal waters west of the Antarctic Peninsula. Proc. Natl Acad. Sci. USA 99 (4), 1790–1795.
Ducklow, H.W., 2008. Long-term studies of the marine ecosystem along the west Antarctic Peninsula. Deep Sea Res. II 55 (18–19), 1945–1948.
Ducklow, H.W., Baker, K., Martinson, D.G., Quetin, L.B., Ross, R.M., Smith, R.C., Stammerjohn, S.E., Vernet, M., Fraser, W., 2007. Marine pelagic ecosystems: the West Antarctic Peninsula. Philos. Trans. R. Soc. B-Biol. Sci. 362 (1477), 67–94.
Gregg, W.W., Casey, N.W., 2004. Global and regional evaluation of the SeaWiFS chlorophyll data set. Remote Sens. Environ. 93 (4), 463–479.
Hall, A., Visbeck, M., 2002. Synchronous variability in the Southern Hemisphere atmosphere, sea ice, and ocean resulting from the annular mode. J. Climate 15 (21), 3043–3057.
Holm-Hansen, O., Riemann, B., 1978. Chlorophyll *a* determination: improvements in methodology. Oikos 30, 438–447.
IOCCG, 2006. Remote sensing of inherent optical properties: fundamentals, tests of algorithms, and applications. In: Lee, Z.P. (Ed.), Reports of the International Ocean-Colour Coordinating Group. IOCCG, Dartmouth, Canada.
Justino, F., Peltier, W.R., 2008. Climate anomalies induced by the Arctic and Antarctic Oscillations: glacial maximum and present-day perspectives. J. Climate 21 (3), 459–475.
Kieber, R.J., Hydro, L.H., Seaton, P.J., 1997. Photooxidation of triglycerides and fatty acids in seawater: implication toward the formation of marine humic substances. Limnol. Oceanogr. 42 (6), 1454–1462.
Kishino, M.T.M., Okami, N., Ichimura, S., 1985. Estimation of the spectral absorption coefficients of phytoplankton in the sea. Bull. Mar. Sci. 37 (2), 634–642.
Kostadinov, T.S., Siegel, D.A., Maritorena, S., Guillocheau, N., 2007. Ocean color observations and modeling for an optically complex site: Santa Barbara Channel, California, USA. J. Geophys. Res. Oceans 112 (C7).

Kudela, R.M., Chavez, F.P., 2004. The impact of coastal runoff on ocean color during an El Nino year in Central California. Deep-Sea Res. Part II-Top. Stud. Oceanogr. 51 (10–11), 1173–1185.
Kwok, R., Comiso, J.C., 2002. Spatial patterns of variability in Antarctic surface temperature: connections to the Southern Hemisphere Annular Mode and the Southern Oscillation. Geophys. Res. Lett. 29 (14).
Lovenduski, N.S., Gruber, N., 2005. Impact of the southern annular mode on Southern Ocean circulation and biology. Geophys. Res. Lett. 32 (11).
Magnuson, A., Harding, L.W., Mallonee, M.E., Adolf, J.E., 2004. Bio-optical model for Chesapeake Bay and the Middle Atlantic Bight. Estuar. Coast. Shelf Sci. 61 (3), 403–424.
Maritorena, S., Siegel, D.A., Peterson, A.R., 2002. Optimization of a semianalytical ocean color model for global-scale applications. Appl. Opt. 41 (15), 2705–2714.
Maritorena, S., d'Andon, O.H.F., Mangin, A., Siegel, D.A., 2010. Merged Satellite Ocean Color Data products using a bio-optical model: characteristics, benefits and issues. Remote Sens. Environ. 114, 1791–1804.
Marrari, M., Hu, C.M., Daly, K., 2006. Validation of SeaWiFS chlorophyll *a* concentrations in the Southern Ocean: a revisit. Remote Sens. Environ. 105 (4), 367–375.
McClain, C.R., 2009. A decade of satellite ocean color observations*. Annu. Rev. Mar. Sci. 1 (1), 19–42.
Meredith, M.P., Murphy, E.J., Hawker, E.J., King, J.C., Wallace, M.I., 2008. On the interannual variability of ocean temperatures around South Georgia, Southern Ocean: forcing by El Niño/Southern Oscillation and the Southern Annular Mode. Deep-Sea Res. Part II-Top. Stud. Oceanogr. 55 (18–19), 2007–2022.
Mitchell, B.G., Holmhansen, O., 1991. Biooptical properties of Antarctic Peninsula waters — differentiation from temperate ocean models. Deep-Sea Res. A-Oceanogr. Res. Pap. 38 (8–9), 1009–1028.
Mitchell, B.G., Brody, E.A., Holmhansen, O., McClain, C., Bishop, J., 1991. Light limitation of phytoplankton biomass and macronutrient utilization in the Southern-Ocean. Limnol. Oceanogr. 36 (8), 1662–1677.
Moore, J.K., Doney, S.C., 2006. Remote sensing observations of ocean physical and biological properties in the region of the Southern Ocean Iron Experiment (SOFeX). J. Geophys. Res. Oceans 111 (C6).
Mopper, K., Zhou, X.L., Kieber, R.J., Kieber, D.J., Sikorski, R.J., Jones, R.D., 1991. Photochemical degradation of dissolved organic-carbon and its impact on the oceanic carbon-cycle. Nature 353 (6339), 60–62.
Nelson, N.B., Siegel, D.A., 2002. Chromophoric DOM in the open ocean. In: Hansell, D.A., Carlson, C.A. (Eds.), Biogeochemistry of Marine Dissolved Organic Matter. Academic Press, San Diego.
Nelson, N.B., Siegel, D.A., Michaels, A.F., 1998. Seasonal dynamics of colored dissolved material in the Sargasso Sea. Deep-Sea Res. Part I-Oceanogr. Res. Pap. 45 (6), 931–957.
Nelson, N.B., Carlson, C.A., Steinberg, D.K., 2004. Production of chromophoric dissolved organic matter by Sargasso Sea microbes. Mar. Chem. 89 (1–4), 273–287.
Nelson, N.B., et al., 2007. Hydrography of chromophoric dissolved organic matter in the North Atlantic. Deep-Sea Res. Part I-Oceanogr. Res. Pap. 54 (5), 710–731.
Ortega-Retuerta, E., Reche, I., Pulido-Villena, E., Agustí, S., Duarte, C.M., 2010. Distribution and photoreactivity of chromophoric dissolved organic matter in the Antarctic Peninsula (Southern Ocean). Marine Chemistry 118, 129–139. doi:10.1016/j.marchem.2009.11.008.
Ortega-Retuerta, E., Duarte, C.M., Ruiz-Halpern, S., Tovar-Sanchez, A., Arrieta, J.M., Reche, I., 2009. Biogeneration of chromophoric dissolved organic matter by bacteria and krill in the Southern Ocean. Limnol. Oceanogr. 54 (6), 1941–1950.
Patterson, K.W., 2000. Contribution of Chromophoric Dissolved Organic Matter to Attenuation of Ultraviolet Radiation in Three Contrasting Coastal Areas. University of California Santa Barbara, Santa Barbara.
Pegau, S., Zaneveld, J.V.R., Mitchell, B., Mueller, G., Kahru, J.L., Wieland, M., Malgorzat, J., Stramska, M., 2003. Inherent Optical Properties: Instruments, Characterizations, Field Measurements and Data Analysis Protocols. NASA.
Pomeroy, L.R., Wiebe, W.J., 2001. Temperature and substrates as interactive limiting factors for marine heterotrophic bacteria. Aquat. Microb. Ecol. 23 (2), 187–204.
Reche, I., Pace, M.L., Cole, J.J., 2000. Modeled effects of dissolved organic carbon and solar spectra on photobleaching in lake ecosystems. Ecosystems 3 (5), 419–432.
Reynolds, R.A., Stramski, D., Mitchell, B.G., 2001. A chlorophyll-dependent semianalytical reflectance model derived from field measurements of absorption and backscattering coefficients within the Southern Ocean. J. Geophys. Res. Oceans 106 (C4), 7125–7138.
Rochelle-Newall, E.J., Fisher, T.R., 2002. Production of chromophoric dissolved organic matter fluorescence in marine and estuarine environments: an investigation into the role of phytoplankton. Mar. Chem. 77 (1), 7–21.
Romera-Castillo, C., Sarmento, H., Alvarez-Salgado, X.A., Gasol, J.M., Marrase, C., 2010. Production of chromophoric dissolved organic matter by marine phytoplankton. Limnol. Oceanogr. 55 (1), 446–454.
Siegel, D.A., Maritorena, S., Nelson, N.B., Hansell, D.A., Lorenzi-Kayser, M., 2002. Global distribution and dynamics of colored dissolved and detrital organic materials. J. Geophys. Res. Oceans 107 (C12). doi:10.1029/2001JC000965.
Siegel, D.A., Maritorena, S., Nelson, N.B., 2005a. Independence and interdependencies among global ocean color properties: reassessing the bio-optical assumption. J. Geophys. Res. Oceans 110 (C7). doi:10.1029/2004JC002527.
Siegel, D.A., Maritorena, S., Nelson, N.B., Behrenfeld, M.J., McClain, C.R., 2005b. Colored dissolved organic matter and its influence on the satellite-based characterization of the ocean biosphere. Geophys. Res. Lett. 32 (20). doi:10.1029/2005GL024310.
Smetacek, V., Nicol, S., 2005. Polar ocean ecosystems in a changing world. Nature 437, 362–368.
Swan, C.M., Siegel, D.A., Nelson, N.B., Carlson, C.A., Nasir, E., 2009. Biogeochemical and hydrographic controls on chromophoric dissolved organic matter distribution in the Pacific Ocean. Deep Sea Res. Part I: Oceanogr. Res. Pap. 56 (12), 2175–2192.
Thompson, D.W.J., Solomon, S., 2002. Interpretation of recent Southern Hemisphere climate change. Science 296 (5569), 895–899.
Toole, D.A., Siegel, D.A., Doney, S.C., 2008. A light-driven, one-dimensional dimethylsulfide biogeochemical cycling model for the Sargasso Sea. J. Geophys. Res. 113.
Vaughan, D.G., Marshall, G.J., Connolley, W.M., Parkinson, C., Mulvaney, R., Hodgson, D.A., King, J.C., Pudsey, C.J., Turner, J., 2003. Recent rapid regional climate warming on the Antarctic Peninsula. Clim. Change 60 (3), 243–274.
Vodacek, A., Blough, N.V., DeGrandpre, M.D., Peltzer, E.T., Nelson, R.K., 1997. Seasonal variation of CDOM and DOC in the Middle Atlantic Bight: terrestrial inputs and photooxidation. Limnol. Oceanogr. 42 (4), 674–686.
Wang, M.H., Shi, W., 2009. Detection of ice and mixed ice-water pixels for MODIS ocean color data processing. IEEE T. Geosci. Remote 47 (8), 2510–2518.
Williamson, C.E., Neale, P.J., Grad, G., De Lange, H.J., Hargreaves, B.R., 2001. Beneficial and detrimental effects of UV on aquatic organisms: Implications of spectral variation. Ecol. Appl. 11 (6), 1843–1857.